The Effect of Impurities on Γ-Alumina Chlorination in a Fluidized Bed Reactor: a CPFD Study

Zahir Barahmand, Chameera Jayarathna and Chandana Ratnayake

September 25, 2021

The Effect of Impurities on γ-Alumina Chlorination in a Fluidized Bed Reactor: A CPFD Study

Zahir Barahmand[1]   Chameera Jayarathna[2]   Chandana Ratnayake[1,2]

[1] Department of Process, Energy and Environmental Technology, University of South-Eastern Norway
zbarahmand@gmail.com
[2] SINTEF Tel-Tek, SINTEF Industry, Porsgrunn, Norway

Abstract

Alumina is one of the most widely used materials today, with a total annual production of millions of tonnes of highly pure alumina. A large portion of this is used to make metal aluminum. Apart from that, a growing amount of alumina is used in ceramics, refractories, catalysts, and various other products. In nature, alumina can be found in different phases. These phases can be transformed into each other in different temperatures. Among these, γ-alumina is used in the chlorination process in the aluminum production industry because of the higher reaction rates. Previously, the chlorination of pure γ-alumina has been considered in the CPFD simulations. Extending previous researches, the present study investigates the effect of seven percent α-alumina impurity on the overall chlorination reaction, bed hydrodynamics, and composition of the outflow of the reactor. Commercial CPFD software Barracuda® v20.1.0 is used for the simulations. The results are compared with the pure γ-alumina simulations, and the results show that the impurity has no considerable effect on the chlorine concentration at the outlet. However, the mass balance of the bed shows an unfavorable accumulation of α-alumina in the fluidized bed reactor.

Keywords: Barracuda, CPFD simulation, α-Alumina chlorination, γ-alumina chlorination, Fluidized bed reactor (FBR),
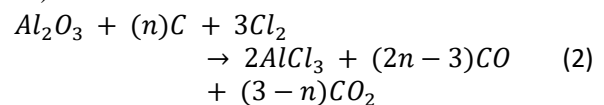
1 Introduction

The Romans called materials with a styptic or astringent flavor "alumen." Impure forms of aluminum sulfate and alum could have been among them naturally occurring in volcanic areas. Term alumina appears to be derived from the mineral alumen (Beckmann, 1846). Alumina is the raw material used for the production of metal Aluminum.

The process which is used almost exclusively in the aluminum industry is the Hall-Héroult process. This process has turned aluminum metal into a commodity product since its invention in 1886 (Kovács et al., 2020). Alumina is dissolved in a cryolite bath in this continuous process, and aluminum is produced by electrolysis. In this cryolite-alumina melt electrolysis, aluminum oxide is dissolved in molten cryolite (Na_3AlF_6) and afterward electrolytically reduced to aluminum at almost 960 °C. Carbon anodes are used in the process, consumed during electrolysis, are resulting in the formation of CO_2. This process suffers from relatively high heat loss from the electrolytic cells and increased CO_2 emissions from the anodes, even though manufacturers have gradually improved their production processes. Besides, the Hall-Héroult process moves down to its potentially lowest energy consumption and CO_2 emissions during decades (Prasad, 2000). The following reaction (2.1) can be the overall reaction of dissolved alumina with carbon to form the products (Thonstad, 2001).

$$\tfrac{1}{2}\,Al_2O_3\,(dissolved)\,+\,\tfrac{3}{4}\,C\,(s) \rightarrow Al\,(l)\,+\,\tfrac{3}{4}\,CO_2\,(g) \tag{1}$$
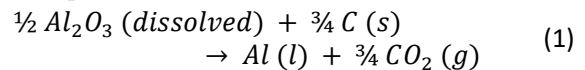
Alternative aluminum processing strategies have been under intense investigation due to the comparatively high energy usage and carbon footprint associated with anode consumption (Thonstad, 2001). In continuation of this, in 1973, an innovative process was introduced by Alcoa Corporation, and it had several advantages compared to the commonly used method (Hall-Héroult) at that time (*National Fuels and Energy Conservation Act, S. 2176*, 1973). Alcoa's process is based on the chlorination of processed aluminum oxide. The chlorination process has the advantages of being more compact and operating at a lower temperature than the Hall-Héroult process, normally 700 °C. Unlike the Hall-Héroult process, which needs pure alumina, one of the main advantages of the chlorination process is the possibility of using impure alumina. The following simplified general reaction can be used to reflect carbothermic chlorination of alumina (Rao & Soleiman, 1986):

$$Al_2O_3\,+\,(n)C\,+\,3Cl_2 \rightarrow 2AlCl_3\,+\,(2n-3)CO\,+\,(3-n)CO_2 \tag{2}$$

where, $1.5 \leq n \leq 3$. The following sequential reactions can explain the carbothermic chlorination of alumina as the reaction progresses with the production of carbon dioxide and carbon monoxide:

$$Al_2O_3\,+\,3CO\,+\,3Cl_2 \rightarrow 2AlCl_3\,+\,3CO_2 \tag{3}$$

$$C\,+\,CO_2 \rightarrow 2CO\,, bounded\ reaction \tag{4}$$
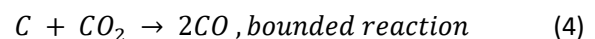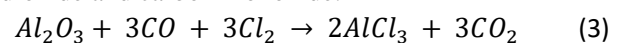
The experimental techniques for obtaining gas-solid contact and extracting gaseous materials containing

AlCl$_3$ and impurity elements are crucial in deciding the chlorination rate.

Experiments of different CO/Cl$_2$ molar ratios revealed that CO/Cl$_2$ = 1 has the highest chlorination rate, and this is clear from overall reactions (3), which involve equimolar concentrations of CO and Cl$_2$ (Gokcen, 1983). The optimal temperature for chlorinating aluminous resources with CO + Cl$_2$ is between 600° and 900°C, with 650 to 750°C being the most expected range. According to (Alder et al., 1977), 600°C could be a reasonable operating temperature for an alumina chlorination fluidized bed. In an industrial chlorination reactor, erosion and chlorination of reactor lining are significantly reduced at lower temperatures. Hence, chlorination at low temperatures tends to be desirable for designers.

Commercial chlorination reactor construction materials must be kept cold enough to prevent being chlorinated. As a result, it seems that externally heated chambers are not feasible. An appropriate series of reactions must be chosen to produce enough heat to keep the internal reactor temperature up while retaining a temperature gradient that allows for a relatively cold and nearly non-reacting wall (Gokcen, 1983).

The Alcoa process's overall chlorination reaction has been introduced by equations (2-4), where solid-phase alumina (mainly Al$_2$O$_3$) reacts with the gaseous chlorine and carbon monoxide at 700 °C. It is vital to know that many alumina particles have different purities and size distribution, affecting the reaction rate.

α-Alumina has outstanding mechanical properties and superb thermal properties at high temperatures; polycrystalline α-alumina is used as a structural ceramic. As a result, this type has much lower reaction rates in the chlorination process. The present study aims to investigate the effect of an impurity (α-alumina) in an industrial γ-alumina chlorination fluidized bed reactor under the isothermal condition at 700 °C. First, some critical information about the stoichiometry of alumina chlorination, reactants, and products is given. Next, the alumina chlorination kinetics for both types have been introduced, which are used from previous studies. In the current study, SOLIDWORKS® has been used for the mechanical design of the fluidized bed reactor, and the reactor model is then simulated/optimized with the use of CFD software called Barracuda VR® version 20.1. At the final step, the results have been compared with the same model reacting pure γ-alumina (Barahmand et al., 2021).

2 Alumina chlorination stoichiometry

The stoichiometry of chlorination of reactants is as reaction (5),

$$Al_2O_3\ (s)\ +\ 3Cl_2\ +\ 3CO \\ \rightarrow\ 2AlCl_3\ +\ 3CO_2 \qquad (5)$$
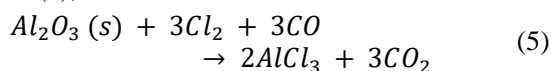
Al$_2$O$_3$: In nature and different thermal conditions, alumina is found in different phases. These phases can be transformed into each other. Table 1 (Aswad, 2012) shows some properties of three main types of alumina. The density of the alpha type is more than other types.

Table 1 Properties of different types of alumina

Type	Envelope Density (kg/m^3)	Melting Temp (°C)
α-alumina	2600	2051
γ-alumina	2100	γ →δ:700-800
θ-alumina	2330	θ →α:1050

AlCl$_3$: because of low vapor pressure (1 atm) at 169.7°C, the gas phase is almost all Al$_2$Cl$_6$ (g). However, during chlorination at high temperatures, both gaseous AlCl$_3$ and Al$_2$Cl$_6$ are present in the process. It has a shallow melting point of about 192°C.

$$2AlCl_3\ \rightleftarrows\ Al_2Cl_3 \qquad (6)$$
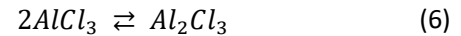
AlCl$_3$ in the gaseous phase is in equilibrium with Al$_2$Cl$_6$. Table 2 shows their volume percentage at different temperatures (Gokcen, 1983).

**Table 2** Volume percentage of AlCl$_3$ and Al$_2$Cl$_6$ in equilibrium

Temperature (K)	600	800	1000	1200
AlCl$_3$ (%)	2.1	35.5	88.4	98.7
Al$_2$Cl$_6$ (%)	97.9	64.5	11.6	1.3

CO and Cl$_2$: At the 1 atm pressure, CO and Cl$_2$ are in equilibrium with phosgene (COCl$_2$). The volume percentage of each in a mixture with different temperatures is given in Table 3 (Gokcen, 1983).

Table 3 Volume percentage of CO + Cl$_2$ and COCl$_2$ in equilibrium

Temperature (K)	800	1000
CO (%)	30.8	48.16
COCl$_2$ (%)	30.8	48.16
Cl$_2$ (%)	38.4	3.68

An equimolar mixture of CO and Cl$_2$ can contain small amounts of COCl$_2$ in the normal temperature range of chlorination. However, This is not an issue because the reaction of alumina with phosgene is faster than an equimolar mixture of CO and Cl$_2$ (Bertóti et al., 1981).

$$Cl_2\ +\ CO\ \rightleftarrows\ COCl_2 \qquad (7)$$
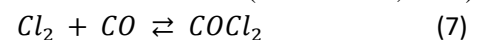
3 Process kinetics

3.1 γ-Alumina chlorination kinetics

In 1981 the temperature and partial pressure dependency and the influence of photo-irradiation of the reactive gases were studied to find reaction rate for γ-alumina chlorination with carbon monoxide and chlorine (Tóth et al., 1982) and phosgene (Bertóti et al., 1981) in different temperatures. To experiment with carbon

monoxide and chlorine, the isothermal TG measurements were taken at temperatures ranging from 327 to 850°C. It has been shown that the reaction conversion and the specific initial reaction rate (R_0) have a significant temperature dependency. The reaction rates for phosgene are higher than the mixture of CO and Cl_2 up to around 920 K, as observed, while the data obtained with both are almost the same as results in (Bertóti et al., 1981). Unlike (Milne, 1976), solid samples have been preheated before chlorination, and as a result, they have been gotten rid of the uncontrolled behavior of the change in the sample's reactivity due to structural changes. The Arrhenius style of specific reaction rate (R_0) is illustrated in Figure 1.
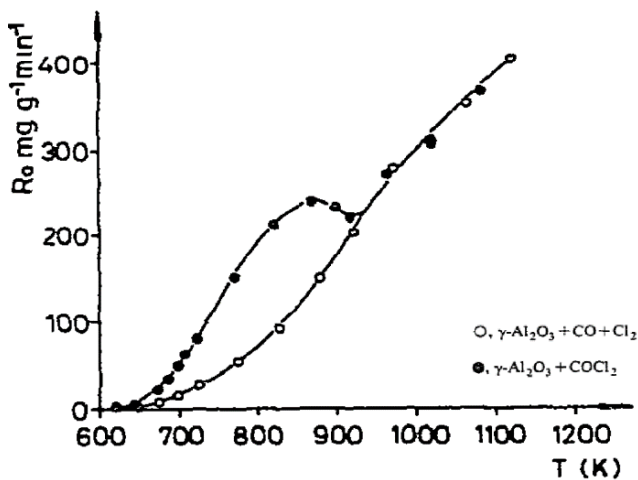

Figure 1. The specific initial reaction rate (R0) vs. temperature (T) in reaction with phosgene (black) and CO+Cl_2 mixture (white) (Tóth et al., 1982)

For the reaction with CO+Cl_2 mixture, the activation energies (E_1) computed by the rate constant of the first-order kinetic equation and initial reaction rate are 106 and 118 kJ/mole. Between temperatures 775-878 K, E_2 is almost half of the E_1 and equal to 56 kJ/mole, and for the range between 920-1123 K, E_3 is the lowest and equal to 23 kJ/mole, indicating that the process at these temperatures is effectively regulated by external mass transfer.

Figure 2 verifies the above-described phenomenon, as the results of an experimental investigation (Milne, 1976) studied chlorination of two different sizes (7.9 mm and 0.125 mm) of γ-alumina with an equimolar mixture of CO and Cl_2. The particle's surface area directly impacts the reaction (Kunii & Levenspiel, 1991). As per the findings of this experiment, it is expected that the fluidized bed's reaction rate will be much quicker than the experiment when very tiny alumina particles are used in the reactor.
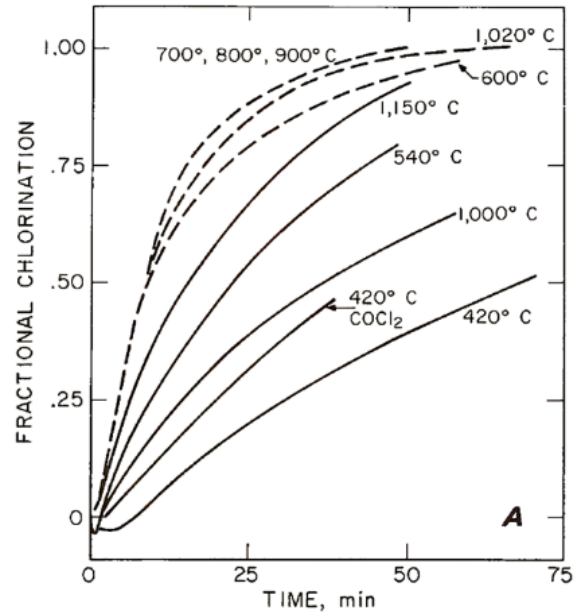

Figure 2. Chlorination of γ-alumina with CO/Cl_2=1. Solid lines are for 9.7 mm particles; broken lines are for 0.125 mm particles (Milne, 1976).

3.2 α-Alumina chlorination kinetics

As (Soleiman & Rao, 1987) reported, the reaction rate and activation energy of the α-alumina in a carbo-chlorination reaction is much lower than that of the γ type. In the range 800-900℃, the activation energy is 32±2.5 kJ/mole. In general,

$$r_{exp} = K\left(P_{cl_2}\right)^{m}(P_{CO})^{n} \qquad (8)$$

where, P_x is the partial pressure of component x, m and n are reaction orders, K is the reaction constant, and r_{exp} is an experimentally calculated reaction rate. Table 4 gives calculated m and n in different temperatures.

Table 4. Reaction orders in different temperatures

	Reaction Temperatures (℃)				
	800	**835**	**870**	**910**	**950**
m	0.71	0.60	0.59	0.56	0.48
n	0.77	0.72	0.66	0.65	0.65

The rate expression for the particular case considered under the experiment considerations can be written as,

$$r_{exp} = \tilde{k}\left(P_{cl_2}\right)(P_{CO}) \qquad (9)$$

where, $\tilde{k}$ is the apparent rate constant in gg^{-1}min^{-1}atm. Table 5 shows the different values for the apparent rate constant,

Table 5. Values of $\tilde{k}$ obtained by regression analysis of r_{exp} vs $\left(P_{cl_2}\right)(P_{CO})$ results

T (℃)	800	835	870	910	950
$\tilde{k}$	0.0234	0.0256	0.0281	0.0313	0.0368
$ln\tilde{k}$	-3.755	-3.665	-3.572	-3.464	-3.302
10000/T	9.3197	9.0253	8.8479	8.4531	8.1766

4 CPFD model

The CPFD method is applied to an industrial alumina chlorination reactor with modified geometry (cylindrical reactor with a section with an extended diameter on top) with a smooth exit on top (Figure 5), and the bed aspect ration (H/D) equal to 2 has been used (Barahmand *et al.*, 2021). The alumina chlorination calculation is three-dimensional, with chemistry in a large industrial reactor at isothermal conditions (700℃). The CPFD method provided a chlorination solution for 3600 seconds. The calculation took 5 days to complete the computation on a single Intel Xeon E5 computer using 55000 cells in total.

An equimolar mixture of CO and Cl_2 enters continuously from the bottom of the reactor, and the products leave the reactor from the top. The initial bed contains mainly γ-alumina with only 7% of $\boldsymbol{\alpha}$-alumina as the impurity. The amount of γ (top) and $\boldsymbol{\alpha}$-alumina (bottom) types are patched in the particle bed as shown in Figure 5 (right). In terms of the concentration, the same percentage of the impurity ($\boldsymbol{\alpha}$-alumina) has been applied to injected solid particles through the feeder (total particle feed is 0.6 kg/s). Specifications of the particles have a crucial role in the fluidized bed hydrodynamics, such as size distribution, sphericity, porosity, and the void fraction of the particle bed. The particle size distribution given in Figure 3 is used for both γ and $\boldsymbol{\alpha}$ alumina types.

Figure 4. Alumina sample under the microscope

It has been observed that this shows a considerable amount of cracked particles (by attrition), which might be created during the process. Based on the approximation guideline (Liang et al., 2016), the cracked particles mostly have sphericity below 0.5, but the sphericity for the not cracked particles could be estimated close to 0.9 (Figure 4). All in all, 0.9 for the average sphericity of this alumina is somewhat optimistic, and finally, 0.7 has been chosen.

The parameters defined for the γ-alumina particles in the simulation are given in Table 6. Except for the envelope density, other parameters are the same in both alumina types. The envelope density of α-alumina has been set to 2600 kg/m³.

Table 6. γ-Alumina Properties

Parameter	Effects on	Used-values
Average diameter	H, R	98 microns
Sphericity	H	0.7
Emissivity	R,HT	0.75
Envelope Density	H	2100 kg/m³
Bulk Density	H	1.19 kg/m³
Diffusion coefficient	R	2.2E-06 cm²/s
Void Fraction	H	0.46

(H: Hydrodynamics, R: Reaction, HT: Heat Transfer)

The WenYu-Ergun drag model (Xie et al., 2018) has been used, and the reaction rate has been set using the information in sections 3.1 and 3.2. The superficial velocity has been set close to the minimum bubbling velocity (0.1 m/s). The pressure boundary in the outlet has been assumed 1 atm.
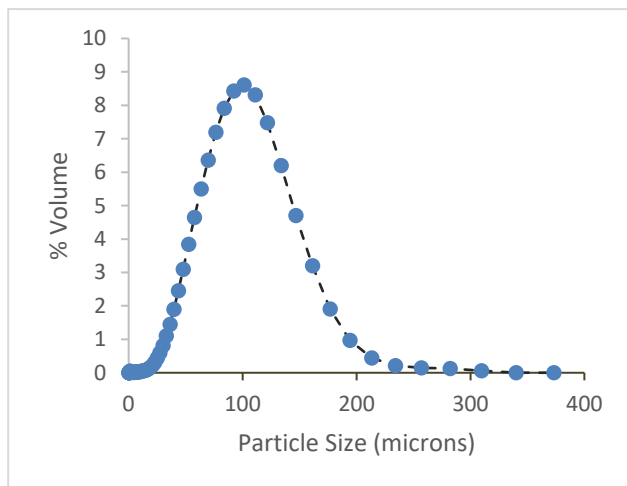

Figure 3. Particle size distribution of the alumina sample

The particle sphericity, envelop density, and bed void fraction cannot be calculated easily and need special measuring apparatus and procedures. However, an extensive range of values has been reported in the literature. To get closer to the acceptable range, an experiment has been done. Finding a reasonable estimation of sphericity, a random sample has been studied under a microscope[1].
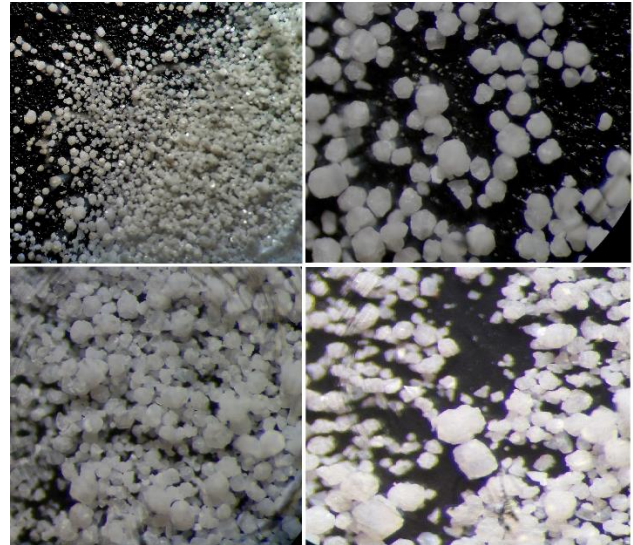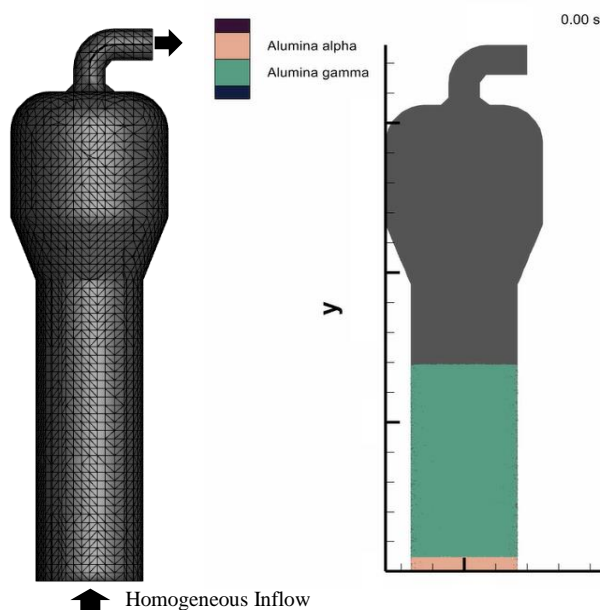
---

[1] Nikon smz745T

Figure 5. Reactor meshed geometry (left), different types of alumina in the initial bed (right)

Figure 6. Different types of alumina particle's distribution after fluidization (left) in steady-state (right)

5   Results and discussion

Comparing the chlorine concentration in the outlet with pure γ-alumina (Barahmand et al., 2021) with the present study confirms that 7% impurity in the alumina sample does not affect reaction conversion. The average chlorine concentration in both cases is below 0.0003 mole/m^3 in the outlet. Although the reaction kinetics clearly shows that the reaction rate for α-alumina is much slower than the γ-alumina, the impurity shows no adverse effect on the Cl_2 concentration in the outlet because the chlorination reaction is rapid. On the other hand, there are more solid particles than needed to react with the gaseous reactants.

Figure 6 shows the α and γ-type alumina particle distribution through the reactor. However, because of the densification, α-alumina is relatively heavier than γ-alumina. After only 700 seconds, it has been distributed homogeneously through the bed.

Studying the particle outflow in the pseudo-steady-state shows that the overall particle escape is 156 g/s, almost one-fourth of the feed. The average escaping rate of α-alumina (from 500 seconds in steady-state) particles has been recorded as only 6 g/s, almost 3.8 percent, while this percent is 7 for the feed. As a result, α-alumina may accumulate inside the reactor. One reason can be the higher density (about 25 percent) of α-alumina. Figure 8 shows that the distribution of the particles leaving the reactor. Almost 97 % of these particles have a mean diameter below 20 microns.
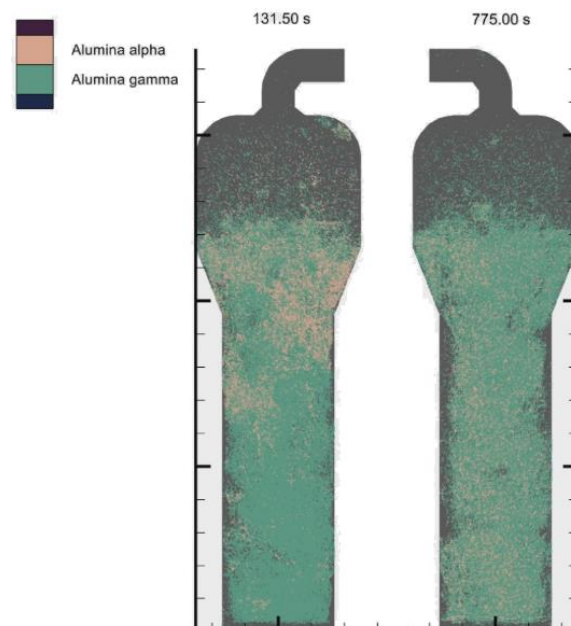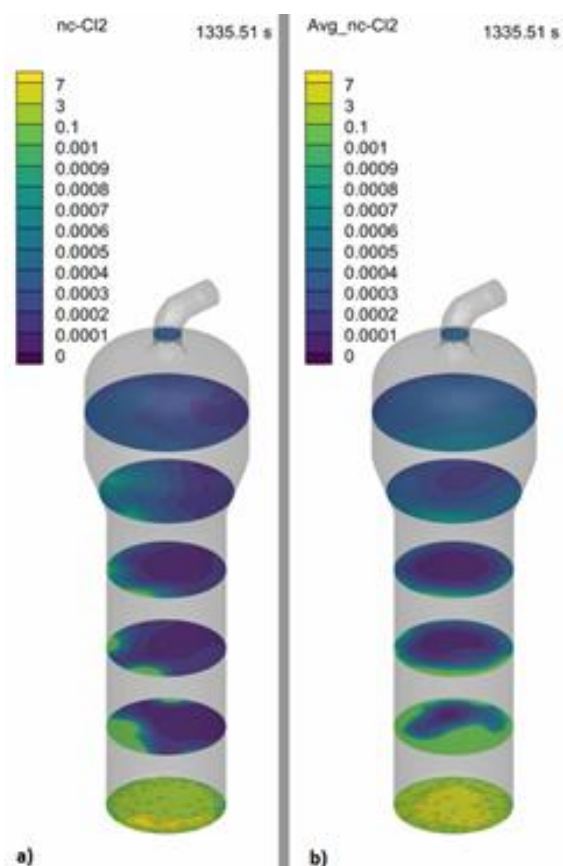

Figure 7. Cl_2 concentration (mole/m^3) in different heights, a) Cl_2 concentration at the specific time, and b) Average Cl_2 concentration in the last 300 seconds.
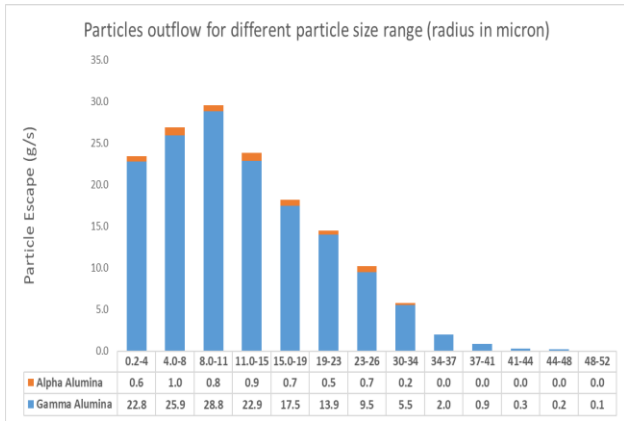
Figure 8. Composition of the particle outflow

Figure 9 and Figure 10 show the size distribution of the different alumina components leaving the reactor. The biggest γ-alumina particle that can leave the system is in the range of 48-52 microns. This value for the α-alumina is in the range of 30-34 microns, emphasizing the higher density of these particles, leading to higher terminal velocity.
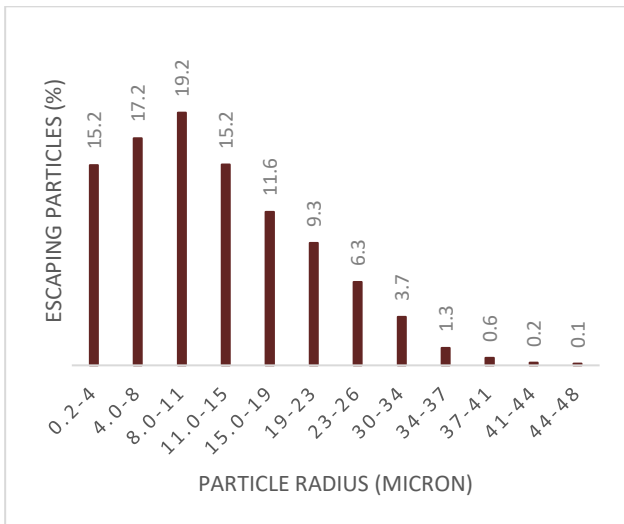

Figure 9. γ-Alumina size distribution in the outlet

The mass balance of the bed shows an unfavorable accumulation of α-alumina in the fluidized bed reactor. During the one-hour simulation period, α-alumina is accumulated at the rate of 5 g/s, and the bed losses γ-alumina at the same rate. Although the alumina inflow rate is constant (0.6 kg/s with a fixed 7 % impurity), α-alumina in the bed is increased, and the overall reaction efficiency of the reactor went down. To minimize the harmful effects of the accumulated α-alumina particles, the particles inside the reactor should be replaced periodically.

An increased amount of non-reactive particles in bed may also increase the particle outflow, but that could be minimized by introducing a proper solid circulation mechanism. However, this may not completely stop the

α-alumina accumulation within the system. Nevertheless, the circulation system for particles can increase the particles' residence time, which may help α-alumina particles reach complete chlorination.
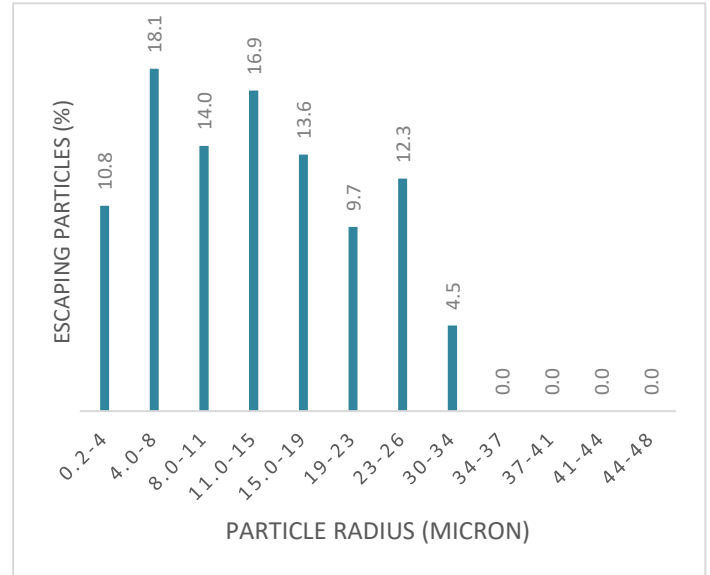

Figure 10. α-Alumina size distribution in the outlet

6 Conclusion

Compared with the model with pure γ-alumina, the results show that, as an impurity, α-alumina does not affect the chlorine concentration at the outlet. The overall particle outflow has become slightly higher in the case of pure γ-alumina. Compared with the α-alumina inflow, which is 7 % of the total inflow, only 3.8 % of the total particle outflow is belongs to α-alumina. In the long run, as a result, α-alumina will be accumulated in the reactor, which is not favorable. In the operating temperature, the reaction rate of α-alumina is much slower, and the accumulation of α-alumina will affect the overall reaction negatively. As remedies, adding a circulation path or speeding up the fluid inside the reactor to a certain point may be helpful, which can be investigated in future works.

References

H. Alder, H. Muller, W. Richarz. Kinetic Study of the Alumina Chlorination with Carbon Monoxide and Chlorine. *Light Metals*, 1977.

Z. Barahmand, C. Jayarathna, and C. Ratnayake. CPFD simulations on a chlorination fluidized bed reactor for aluminum production: An optimization study. *In Proceedings - 1st SIMS EUROSIM Conference on Modelling and Simulation*, Finland, 2021.

J. Beckmann. *History of Inventions, Discoveries, and Origins*. H.G. Bohn, 1846.

I. Bertóti, A. Tóth, T. Székely, and I. Pap. Kinetics of γ-alumina chlorination by phosgene. *Thermochimica Acta*, *44*(3), 325–331, 1981. doi:10.1016/0040-6031(81)85025-3

N. Gokcen. *Rates of chlorination of aluminous resource*, pages 28. U.S. Department of the Interior, Bureau of Mines, 1983.

A. Kovács, C. Breward, K. Einarsrud, S. Halvorsen, E. Nordgård-Hansen, E. Manger, A. Münch, and J. Oliver. A heat and mass transfer problem for the dissolution of an alumina particle in a cryolite bath. *International Journal of Heat and Mass Transfer*, *162*, 120232, 2020. doi:10.1016/j.ijheatmasstransfer.2020.120232

D. Kunii and O. Levenspiel. *Fluidization Engineering*. Butterworth-Heinemann, 1991.

F. Liang, M. Sayed, G. Al-Muntasheri, F. Chang, and L. Li. A comprehensive review on proppant technologies. *Petroleum*, *2*(1), 26–39, 2016. doi:10.1016/j.petlm.2015.11.001

J. Milne. The chlorination of alumina and bauxite with chlorine and carbon monoxide. *Proc Aust Inst Min Metall*, *260*, 23–31, 1976.

National Fuels and Energy Conservation Act, S. 2176, U.S. Government Printing Office, 1973.

S. Prasad. Studies on the Hall-Heroult aluminum electrowinning process. *Journal of the Brazilian Chemical Society*, *11*, 245–251, 2000. doi:10.1590/S0103-50532000000300008

Y. Rao, and M. Soleiman. *Alumina chlorination* (United States Patent No. US4565674A), 1986.

M. Soleiman and Y. Rao. Kinetics and Mechanism of Chlorination of Alumina Grains with He–CO–Cl2 Gas Mixtures—I. Experimental. *Canadian Metallurgical Quarterly*, *26*(3), 207–215, 1987. doi: 10.1179/cmq.1987.26.3.207

J. Thonstad. *Aluminum Electrolysis: Fundamentals of the Hall-Héroult Process*. Aluminium-Verlag, 2001.

A. Tóth, I. Bertóti and T. Székely. Kinetics of γ-alumina chlorination by carbon monoxide and chlorine. *Thermochimica Acta*, *52*(1), 211–215, 1982. doi: 10.1016/0040-6031(82)85198-8

J. Xie, W. Zhong and A. Yu. MP-PIC modeling of CFB risers with homogeneous and heterogeneous drag models. *Advanced Powder Technology*, *29*(11), 2859–2871, 2018. doi: 10.1016/j.apt.2018.08.007